Engineering Turbulence Modelling and Experiments 4
Proc. 4th Int. Symp. on Engineering Turbulence Modelling and Measurements, Ajaccio, F, 24–26 May 1999
W. Rodi and D. Laurence (Eds.), Elsevier Science Ltd. Amsterdam

Consistent modelling of fluctuating temperature-gradient-velocity-gradient correlations for natural convection

M. Wörner, Q.-Y. Ye† and G. Grötzbach

Forschungszentrum Karlsruhe, Institut für Reaktorsicherheit, Postfach 3640,
D-76021 Karlsruhe, Germany

A model is proposed for the buoyant production term in the dissipation rate equation of turbulence kinetic energy and the molecular sink term in the turbulent heat flux equation. Based on an analytical decomposition by the two-point correlation technique the model consists of an inhomogeneous and a homogeneous part. The inhomogeneous part involves the Laplacian operator of the turbulent heat flux and needs no further modelling. For the homogeneous part a model is derived which incorporates Pr/R as key parameter, where Pr is the Prandtl number and R is the ratio of thermal to mechanical turbulent time scales. The model is shown to obey the correct wall-limiting behaviour without further wall corrections. Comparisons with DNS data for Rayleigh Bénard convection in air and sodium and for convection in an internally heated fluid layer confirm its excellent near-wall performance for a wide range of Prandtl numbers. Utilising these DNS data, the performance of the model in the bulk region is improved by slightly modifying the homogeneous part of the model.

1. INTRODUCTION

In nuclear engineering, knowledge of the heat transfer capabilities of buoyant flows is of importance for a variety of applications. Examples related to reactor safety are the passive decay heat removal by natural convection, the in-vessel cooling of a decay-heated pool of molten core material, and, supposed the vessel fails, the long-term sump cooling of the core melt by a recirculating water layer, driven by natural convection. For all these applications, computational fluid dynamics (CFD) is an important tool to explore the velocity and temperature field and extend the safety capabilities. In engineering CFD codes, turbulent momentum and heat transfer are modelled by statistical turbulence closures, which need to be validated and improved to be reliably applicable to strongly buoyant flows.

In the present paper, we focus our attention on two terms which are of importance in statistical modelling of buoyant flows: (i) the buoyant production term $P_{\varepsilon b}$ in the dynamic equation for the dissipation rate ε of turbulence kinetic energy $k = \overline{u_l u_l}/2$ and (ii) the

†Present address: Fraunhofer IPA, Nobelstraße 12, D-70569 Stuttgart, Germany

dissipation term $\varepsilon_{\theta i}$ in the dynamic equation for the turbulent heat flux $\overline{\theta u_i}$. Here, u_i and θ denote the fluctuating velocity and temperature. Introducing the correlation

$$\Upsilon_i = \overline{\frac{\partial \theta}{\partial x_l}\frac{\partial u_i}{\partial x_l}} \tag{1}$$

both terms of interest can be expressed as

$$P_{\varepsilon b} = -2\nu\beta g_i \Upsilon_i, \quad \varepsilon_{\theta i} = (\nu + \kappa)\Upsilon_i, \tag{2}$$

where ν= kinematic viscosity, β= thermal expansion coefficient, κ=thermal diffusivity, and $\vec{g} = (0, 0, -g)$ is the gravity vector.

In Ye et al. [8], where the two-point correlation technique and the invariant theory are used to develop models for the ε-equation for natural convection, also a model for $P_{\varepsilon b}$ was obtained as a preliminary result by using direct numerical simulation (DNS) data. This model together with the consistent model for $\varepsilon_{\theta i}$ [9] was implemented in the engineering CFD code FLUTAN [6]. Calculations for the buoyant flow along a heated vertical plate were performed and compared with experimental results. The models of [8] and [9] clearly yielded improved results as compared to standard models for both terms. Models for $\varepsilon_{\theta i}$ were also recently proposed by Dol et al. [2] and Shikazono & Kasagi [4].

In the present paper, the development of the model proposed in [8] for $P_{\varepsilon b}$ is put on an analytical and physical basis. Furthermore, the analysis is extended to develop a consistent closure relation for both, $P_{\varepsilon b}$ and $\varepsilon_{\theta i}$ which adequately accounts for the Prandtl number $Pr = \nu/\kappa$, turbulence level, and wall effects.

2. Development of model

The turbulent dissipation rate ε can analytically be decomposed by the two-point correlation technique [1] in an inhomogeneous and a homogeneous part [3]:

$$\varepsilon = \nu\overline{\frac{\partial u_s}{\partial x_l}\frac{\partial u_s}{\partial x_l}} = \underbrace{\frac{1}{4}\nu\Delta_x\overline{u_s u_s}}_{inhomogeneous} \underbrace{-\nu(\Delta_\xi \overline{u_s u_s'})_0}_{homogeneous} = \frac{1}{2}\nu\Delta_x k + \varepsilon_h. \tag{3}$$

Here, $\Delta_x = \partial^2/\partial x_l \partial x_l$ is the Laplace operator with respect to the variable x; ξ represents a local coordinate system relative to two arbitrary points (see [1]). The prime $'$ in Eq. (3) indicates a value for the two-point correlation function and the subscript $_0$ represents the zero separation $\xi = 0$ between the two points. Similar to ε, Ye et al. [8] used the two-point correlation technique to decompose Υ_i:

$$\Upsilon_i = \overline{\frac{\partial \theta}{\partial x_l}\frac{\partial u_i}{\partial x_l}} = \underbrace{\frac{1}{4}\Delta_x\overline{\theta u_i}}_{\Upsilon_{i,ih}} \underbrace{-\frac{1}{2}[(\Delta_\xi \overline{\theta u_i'})_0 + (\Delta_\xi \overline{u_i \theta'})_0]}_{\Upsilon_{i,h}} = \Upsilon_{i,ih} + \Upsilon_{i,h}. \tag{4}$$

In correspondence to Eq. (3) $\Upsilon_{i,ih}$ is denoted as the inhomogeneous and $\Upsilon_{i,h}$ as the homogeneous part of Υ_i. While the term $\Upsilon_{i,ih}$ is known by second moment closure of the turbulent heat flux, only the term $\Upsilon_{i,h}$ needs to be modelled for closure of $P_{\varepsilon b}$ and $\varepsilon_{\theta i}$. The advantages of the above decomposition will become clear in this paper. At the moment we only note that $\Upsilon_{i,ih}$ will adequately account for wall effects.

In deriving a closure for $\Upsilon_{i,h}$ we proceed similar to Shikazono & Kasagi [4] who developed a model for $\varepsilon_{\theta i}$. We define a correlation coefficient for Υ_i and relate it to the correlation coefficient for the turbulent heat flux via a functional coefficient $\mathcal{C}$ which has to be determined:

$$\frac{\overline{\frac{\partial\theta}{\partial x_l}\frac{\partial u_i}{\partial x_l}}}{\sqrt{\left(\frac{\partial\theta}{\partial x_l}\right)^2}\sqrt{\left(\frac{\partial u_{(i)}}{\partial x_l}\right)^2}} \simeq \mathcal{C}\frac{\overline{\theta u_i}}{\sqrt{\overline{\theta^2}}\sqrt{u_{(i)}^2}}. \tag{5}$$

We note the definition of the thermal variance dissipation rate

$$\varepsilon_\theta = \kappa\overline{\frac{\partial\theta}{\partial x_l}\frac{\partial\theta}{\partial x_l}} = \kappa\overline{\left(\frac{\partial\theta}{\partial x_l}\right)^2} \tag{6}$$

and assume that the ratio of kinetic energy to dissipation rate of velocity component i equals the ratio of the total turbulence kinetic energy to total dissipation rate:

$$\frac{\overline{u_{(i)}^2}}{\overline{\left(\frac{\partial u_{(i)}}{\partial x_l}\right)^2}} \simeq \frac{2k}{\frac{\varepsilon}{\nu}}. \tag{7}$$

Making use of definition (6) and approximation (7) and introducing the ratio of thermal to mechanical turbulence time scale

$$R = \frac{\overline{\theta^2}}{2\varepsilon_\theta}\frac{\varepsilon}{k}, \tag{8}$$

we can rewrite (5) to yield

$$\Upsilon_i \simeq \frac{\mathcal{C}}{2\sqrt{\nu\kappa R}}\frac{\varepsilon}{k}\overline{\theta u_i}. \tag{9}$$

In their model for $\varepsilon_{i\theta}$ Shikazono & Kasagi [4] introduced two rather complicated wall functions to account for wall effects. In the present approach, the wall effects in modelling Υ_i are already taken into account by the inhomogeneous part of decomposition (4), i.e. by $\Upsilon_{i,ih}$. To model the homogeneous part $\Upsilon_{i,h}$ we make use of (9) but replace Υ_i by $\Upsilon_{i,h}$ and the total dissipation rate ε by the homogeneous one, $\varepsilon_h = \varepsilon - \frac{1}{2}\nu\Delta_x k$. For the moment we leave open whether R defined by Eq. (8) involving the total dissipation rates shall be used, or whether the homogeneous dissipation rates shall be involved, i.e.

$$R_h = \frac{\overline{\theta^2}}{2\varepsilon_{\theta h}}\frac{\varepsilon_h}{k}, \tag{10}$$

where $\varepsilon_{\theta h} = \varepsilon_\theta - \frac{1}{4}\kappa\Delta_x\overline{\theta^2}$. With R_Υ beeing either R or R_h we obtain

$$\Upsilon_{i,h} \simeq \frac{\mathcal{C}}{2\sqrt{\nu\kappa R_\Upsilon}}\frac{\varepsilon_h}{k}\overline{\theta u_i}. \tag{11}$$

This eventually results in our basic model for $P_{\varepsilon b}$ and $\varepsilon_{\theta i}$:

$$P_{\varepsilon b}^* = -\frac{1}{2}\nu\beta g_i\frac{\partial\overline{\theta u_i}}{\partial x_l\partial x_l} - \beta g_i\mathcal{C}\sqrt{\frac{Pr}{R_\Upsilon}}\frac{\varepsilon_h}{k}\overline{\theta u_i}, \tag{12}$$

$$\varepsilon^*_{\theta i,b} = \frac{1}{4}(\nu+\kappa)\frac{\partial\overline{\theta u_i}}{\partial x_l \partial x_l} + \frac{1}{2}\mathcal{C}\left(1+\frac{1}{Pr}\right)\sqrt{\frac{Pr}{R_\Upsilon}}\frac{\varepsilon_h}{k}\overline{\theta u_i} = \varepsilon^*_{\theta i,ih} + \varepsilon^*_{\theta i,hb}. \tag{13}$$

Beside the selection of R_Υ also the functional coefficient $\mathcal{C}$ has to be determined. To do so, in the next section the near-wall behaviour of the above basic model is analysed. In a second step, DNS data will be used to determine $\mathcal{C}$. Below, however, we first compare our basic model with the model of Ye et al. [8] proposed for $P_{\varepsilon b}$ and $\varepsilon_{\theta i}$ [9]:

$$P^*_{\varepsilon b,Ye} = -\frac{1}{2}\nu\beta g_i \frac{\partial\overline{\theta u_i}}{\partial x_l \partial x_l} - \beta g_i \left(\frac{Pr}{R}\right)^{0.7}\frac{\varepsilon_h}{k}\overline{\theta u_i}, \tag{14}$$

$$\varepsilon^*_{\theta i,Ye} = \frac{1}{4}(\nu+\kappa)\frac{\partial\overline{\theta u_i}}{\partial x_l \partial x_l} + \frac{1}{2}\left(1+\frac{1}{Pr}\right)\left(\frac{Pr}{R}\right)^{0.7}\frac{\varepsilon_h}{k}\overline{\theta u_i}, \tag{15}$$

where the term $(Pr/R)^{0.7}$ was obtained by fitting DNS data. We see, that (12) and (14) and (13) and (15) are quite similar and will be identical for $R_\Upsilon = R$ and $\mathcal{C} = (Pr/R)^{0.2}$.

3. Near-wall behaviour of basic model

The wall-limiting behaviour of the basic model can be evaluated by expanding the temperature and velocity fluctuations near the wall:

$$\theta = a_\theta + b_\theta x_3 + c_\theta x_3^2 + d_\theta x_3^3 + \cdots, \tag{16}$$

$$u_i = a_i + b_i x_3 + c_i x_3^2 + d_i x_3^3 + \cdots, \tag{17}$$

where x_3 is the wall-normal coordinate. Here, we consider no-slip boundary conditions ($a_i = 0$), an incompressible fluid ($b_3 = 0$) and isothermal walls ($a_\theta = 0$). By this, we obtain the limiting behaviour

$$\overline{\theta u_3} = b_\theta c_3 x_3^3 + \cdots, \quad \Upsilon_3 = \overline{\frac{\partial\theta}{\partial x_l}\frac{\partial u_3}{\partial x_l}} = 2 b_\theta c_3 x_3 + \cdots. \tag{18}$$

For the near-wall behaviour of the analytical term $\Upsilon_{3,h}$ it follows

$$\Upsilon_{3,h} = \Upsilon_3 - \Upsilon_{3,ih} = (2 b_\theta c_3 x_3 + \cdots) - (\frac{6}{4} b_\theta c_3 x_3 + \cdots) = \frac{1}{2} b_\theta c_3 x_3 + \cdots. \tag{19}$$

To determine the wall-limiting behaviour of our model for $\Upsilon_{3,h}$ we consider the wall-limiting behaviour of the individual variables on the r.h.s. of Eq. (11):

$$\varepsilon_h = \frac{\nu}{2}(b_1^2 + b_2^2) + \cdots,\ k = \frac{1}{2}(b_1^2 + b_2^2)x_3^2 + \cdots,\ \overline{\theta^2} = b_\theta^2 x_3^2 + \cdots,\ \varepsilon_{\theta h} = \frac{\kappa}{2} b_\theta^2 + \cdots. \tag{20}$$

Thus, we obtain the well known result

$$R = Pr + \cdots, \quad R_h = Pr + \cdots, \tag{21}$$

which is valid only for isothermal walls. Introducing these results in Eq. (11) we get

$$\Upsilon_{3,h} = \frac{\mathcal{C}}{2\sqrt{\nu\kappa(\frac{\nu}{\kappa}+\cdots)}}\frac{\frac{\nu}{2}(b_1^2+b_2^2)+\cdots}{\frac{1}{2}(b_1^2+b_2^2)x_3^2+\cdots}\cdot(b_\theta c_3 x_3^3 + \cdots) = \frac{\mathcal{C}}{2} b_\theta c_3 x_3 + \cdots. \tag{22}$$

To establish the correct near-wall behaviour of model (11), the comparison with Eq. (19) requires the wall-limiting behaviour of the functional coefficient $\mathcal{C}$ to be

$$\mathcal{C} = 1 + \cdots. \tag{23}$$

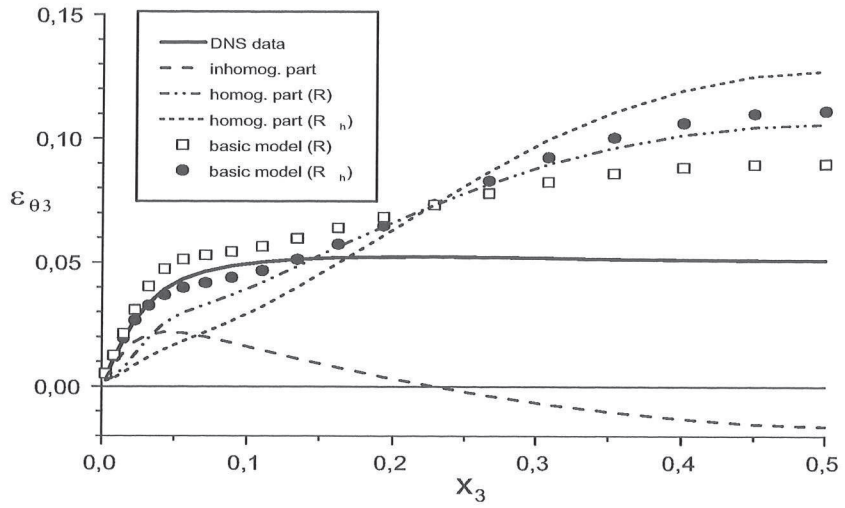

Figure 1. $\varepsilon_{\theta 3}$ for Rayleigh Bénard convection in sodium ($Pr = 0.006, Ra = 12,000$).

4. Comparison of basic model with DNS data

In this section we investigate the performance of the basic model for $\varepsilon_{\theta 3}$ with R_Υ beeing either R or R_h and $C = 1$ by comparison with DNS data. For this purpose, all turbulence quantities appearing on the r.h.s. of Eq. (13) are taken from the DNS database. Two types of natural convection in a horizontal layer bounded by isothermal top and bottom walls are considered. For the Rayleigh Bénard convection, where the lower wall is heated and the upper wall is cooled, a series of simulations has been performed with the TURBIT code at the Research Centre Karlsruhe [10]. The fluids investigated encompass sodium ($Pr = 0.006$), mercury ($Pr = 0.025$), and air ($Pr = 0.71$) and cover a wide range of Prandtl numbers. In this paper the DNS data for sodium at $Ra = 12,000$ and for air at $Ra = 630,000$ are utilised. The Rayleigh number is given by $Ra = u_0^2 D/(\nu\kappa)$, where D is the channel height, $u_0 = \sqrt{g\beta\Delta T D}$ is the buoyant velocity scale, and ΔT is the overall temperature difference. The second type of natural convection is a fluid layer heated internally by a volumetric heat source q_v. Both walls have the same temperature and the fluid is over a wide area stratified thermally stable. The direct numerical simulations, documented in [7], are for $Pr = 7$ and internal Rayleigh numbers up to $Ra_I = 10^9$, where $Ra_I = (g\beta q_v D^5)/(\nu\kappa\lambda)$ with λ=thermal conductivity. Here, we use the DNS data for $Ra_I = 10^8$. In the present paper all data displayed in Figures are dimensionless; the normalisation is by D, u_0, and ΔT.

In Figure 1 we analyse the perfomance of the basic model for Rayleigh Bénard convection in liquid sodium for $R_\Upsilon = R$ and $R_\Upsilon = R_h$. Because of symmetry, only the lower half of the channel is displayed. It appears, that the inhomogeneous part is of importance in the entire channel. The homogeneous part is predominant in the channel centre. In the near wall region we find a good agreement of the basic model with the DNS data if $R_\Upsilon = R_h$ is used. In the channel centre the discrepancy between the basic model and the DNS data is considerable. This holds for both, $R_\Upsilon = R$ and $R_\Upsilon = R_h$, where the latter performs somewhat worse. Due to its superior wall-behaviour we choose $R_\Upsilon = R_h$.

To investigate the influence of Prandtl number and turbulence level, we show in Figure

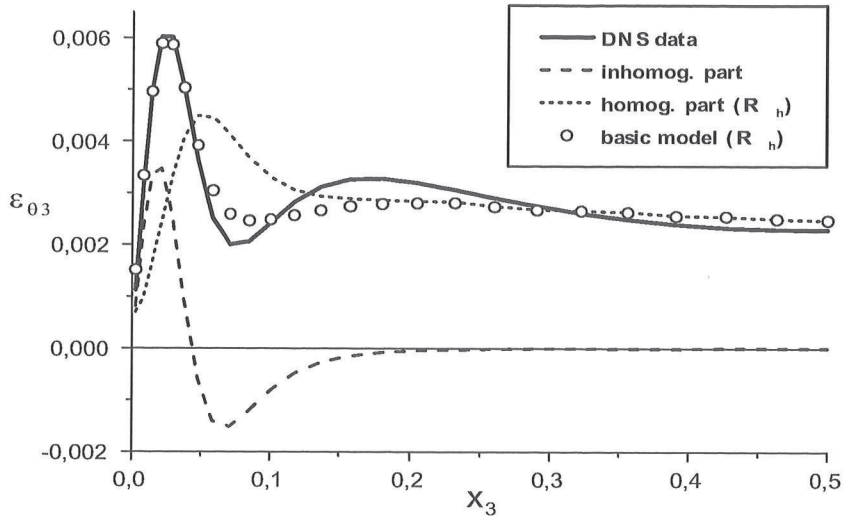

Figure 2. $\varepsilon_{\theta 3}$ for Rayleigh Bénard convection in air ($Pr = 0.71, Ra = 630,000$).

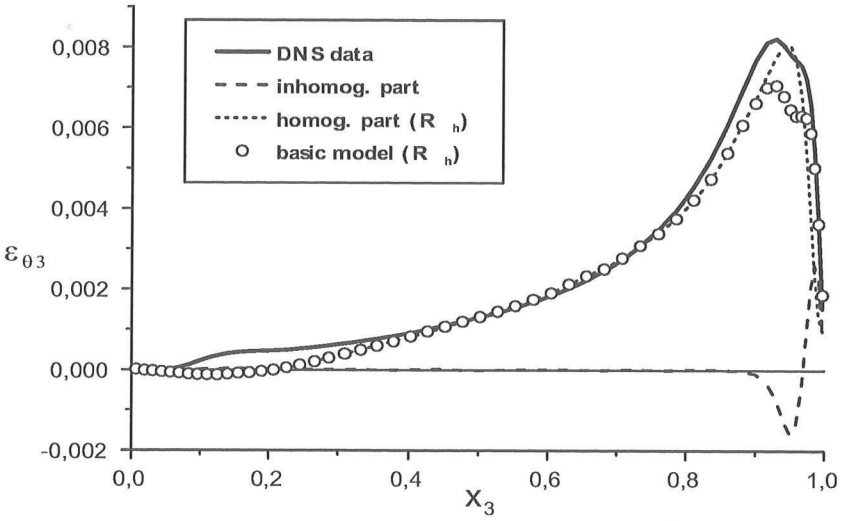

Figure 3. $\varepsilon_{\theta 3}$ for internally heated convection ($Pr = 7, Ra_I = 10^8$).

2 the perfomance of the basic model for Rayleigh Bénard convection in air. The inhomogeneous part of the model is predominant inside the thermal boundary layer, but zero in the channel centre. This is because the bulk region is isothermal and the vertical turbulent heat flux takes a spatially constant value. The basic model for the homogeneous part yields an almost constant value in the bulk region. Figure 2 shows an excellent agreement between the basic model and the DNS data near the wall, while the performance in the channel centre is also good, but may be further improved.

In Figure 3 a comparison of the basic model with DNS data for internally heated convection and $Pr = 7$ is given. The profiles are not symmetric, thus the complete channel is shown. Again, we find a good agreement for both boundary layers. In the region $0.1 \leq x_3 \leq 0.25$ a negative value of $\varepsilon_{\theta 3}$ is predicted by the model, which is not

realistic. This failure can directly be attributed to the linear relation between $\varepsilon^*_{\theta 3,hb}$ and $\overline{\theta u_3}$. Indeed, the DNS data show that for $0.1 \leq x_3 \leq 0.25$ the vertical turbulent heat flux is negative. While for $0.35 \leq x_3 \leq 0.8$ the model again performs well, it somewhat underpredicts the DNS data in region $0.8 \leq x_3 \leq 0.95$.

From these results we conclude, that the model reproduces the DNS data near the wall very well due to the correct limiting behaviour. In the bulk region there is a need and certain potential for further improvement. We therefore modify the homogeneous part of the model, since this is the predominant contribution far from walls.

5. Fine tuning of homogeneous part of model by DNS data

While we want to improve the performance of the model in the channel centre, we do not want to weaken its good performance near the walls. Therefore, the correct wall limiting behaviour of the model must be preserved. This requires a limiting behaviour of $\mathcal{C}$ as defined by Eq. (23). Thus, the possibilities of tuning the model without changing the correct wall behaviour are rather limited.

The unsatisfactory performance of the basic model for sodium in the channel centre may be attributed to the small Prandtl number and low turbulence level. The correlation between fluctuating temperature-gradient and fluctuating velocity-gradient may be expected to be maximised when the thermal turbulence time scale is "in phase" with the mechanical one, i.e. $R \approx 1$. For very small fluid Prandtl numbers and low turbulence levels, however, the thermal turbulence time scale is much smaller than the mechanical one and $R \ll 1$. This may explain why the basic model overestimates $\varepsilon_{\theta 3}$ in sodium, as well as in mercury (the results are not shown here). We therefore identify the key parameter for fine tuning of the model by R or R_h. Because we want to prevail the correct wall-limiting behaviour of the basic model, we perform modifications not in terms of R_h or R, but by the ratio Pr/R_h or Pr/R, respectively. A reasonable ansatz which is in accordance with the requirement of Eq. (23) is of the form

$$\mathcal{C} = \left(\frac{Pr}{R_h}\right)^a \quad \text{or} \quad \mathcal{C} = \left(\frac{Pr}{R}\right)^a . \tag{24}$$

The exponent a may be a function of Prandtl number and, to account for the influence of the turbulence level, of the sum of turbulence Reynolds and Peclet number:

$$a = a(Pr, Re_t + Pe_t), \tag{25}$$

where $Re_t = k^2/(\nu\varepsilon)$ and $Pe_t = Pr \cdot Re_t$. Here we take for simplicity $a = a(Pr)$. The investigation of the influence of the turbulence level requires the analysis of DNS data for a certain Prandtl number at various Rayleigh numbers. This will be done in future work.

In Figure 4 the profiles of Pr/R and Pr/R_h are shown for the simulation with sodium. In addition, the profile of the function $f = (\varepsilon_{\theta 3} - \varepsilon^*_{\theta 3,ih})/\varepsilon^*_{\theta 3,hb}$ is displayed, where $\mathcal{C} = 1$ is used in $\varepsilon^*_{\theta 3,hb}$. If we manage to construct a function $\mathcal{C}$ which meets the profile of f, then a model is obtained which exactly agrees with the DNS data. From Figure 4 it is evident that this is an impossible task, because near the wall f tends to zero while for the coefficient $\mathcal{C}$ we require near the wall $\mathcal{C} \to 1$. Comparing the different profiles in Figure 4 we find, that both f and Pr/R show a local maximum while Pr/R_h does not. A relation

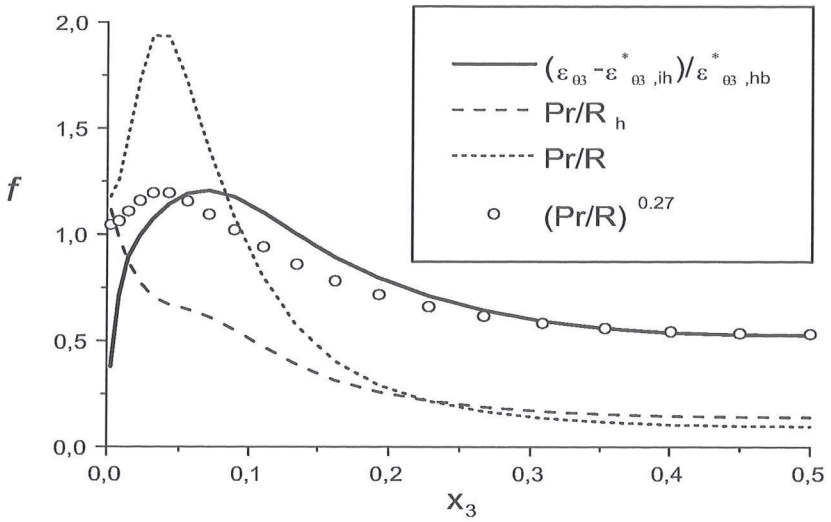

Figure 4. Determination of $\mathcal{C}$ for Rayleigh Bénard convection in sodium.

of type $\mathcal{C} = (Pr/R_h)^a$ is thus unsuited to approximate the profile of f. Therefore, we use Pr/R. The best fit to f in the central region of the channel is obtained with $a = 0.27$, see Figure 4. However, with the exponential ansatz (24) it is not possible to shift the vertical position of the maximum of $\mathcal{C}$ in such a way that its location coincides with that of f.

In Figure 5 we compare the modified model

$$\varepsilon^*_{\theta i} = \frac{1}{4}(\nu + \kappa)\frac{\partial \overline{\theta u_i}}{\partial x_l \partial x_l} + \frac{1}{2}\left(1 + \frac{1}{Pr}\right)\left(\frac{Pr}{R}\right)^a \sqrt{\frac{Pr}{R_h}}\frac{\varepsilon_h}{k}\overline{\theta u_i} \tag{26}$$

for $i = 3$ and $a(Pr = 0.006) = 0.27$ with DNS data for liquid sodium. We now find a much better agreement with the DNS data than was obtained with the basic model. For $0.08 \leq x_3 \leq 0.3$ the agreement is still not fully satisfactory. We note that not having matched f near the wall is not really relevant, because there the contribution of the homogeneous part of the model is small as compared to the inhomogeneous part. In Figure 5 a comparison with the model of Ye et al. [9] is also given. It can be seen that the use of $R_\Upsilon = R_h$ in the present study is superior to $R_\Upsilon = R$ chosen in Eq. (15).

In Figure 6 we compare the modified model with the value $a = 0.27$ optimized for sodium with the DNS data for Rayleigh Bénard convection in air. Again a clear improvement is obtained by the modified model without trying to further optimize a. A quite similar profile is predicted by the model of Ye et al., Eq. (15).

As discussed above, for internally heated convection the basic model underpredicts the DNS data for $\varepsilon_{\theta 3}$ in region $0.8 \leq x_3 \leq 0.95$. As it is shown in Figure 7, the modified model with $a = 0.27$ overpredicts the DNS data. The same holds for the model of Ye et al. [9]. In fact, for internally heated convection the profiles of R and R_h are nearly identical. Therefore our modified model would almost agree with the Ye et al. model for $a = 0.2$. We obtain the best fit with the DNS data for internally heated convection when the rather low value $a = 0.09$ is choosen, see Figure 7. This indicates that $a(Pr)$ is decreasing with increasing Prandtl number and approaches zero. This would effectively result in $\mathcal{C} \to 1$ in the entire channel and the basic model is obtained. However, the clarification of the functional relationship $a(Pr)$ requires further more detailed investigations.

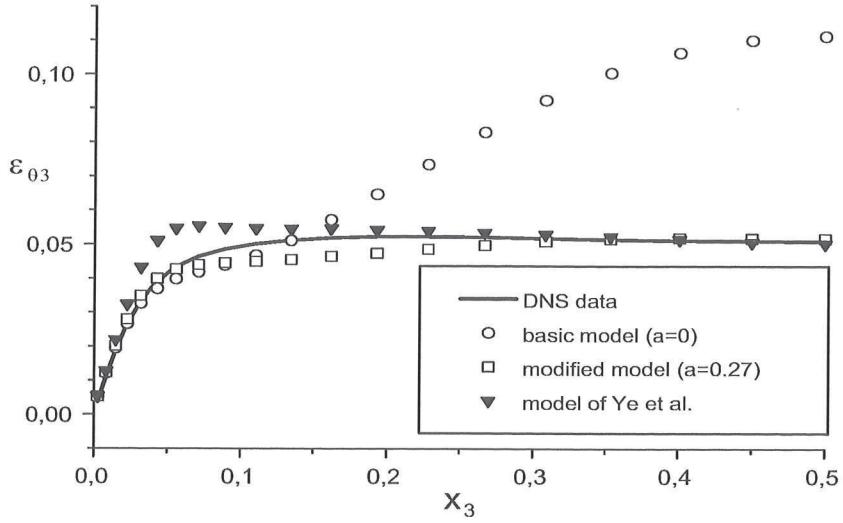

Figure 5. Comparison of models for $\varepsilon_{\theta 3}$ for Rayleigh Bénard convection in sodium.

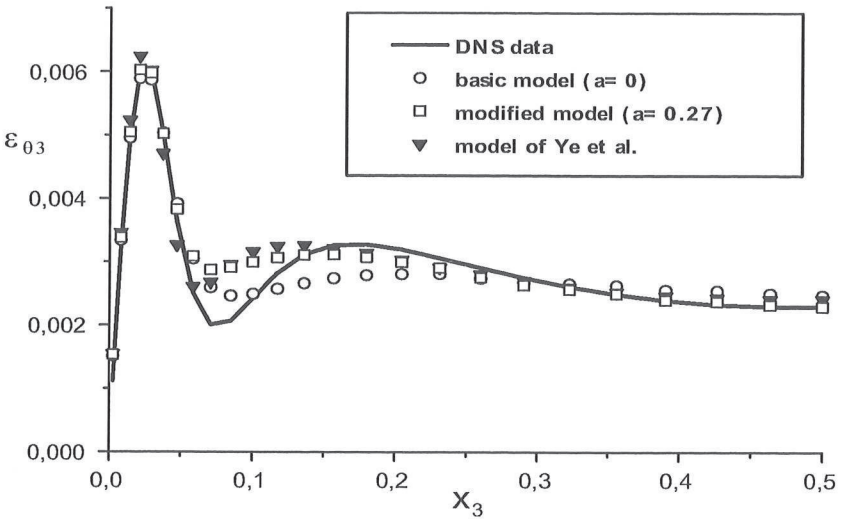

Figure 6. Comparison of models for $\varepsilon_{\theta 3}$ for Rayleigh Bénard convection in air.

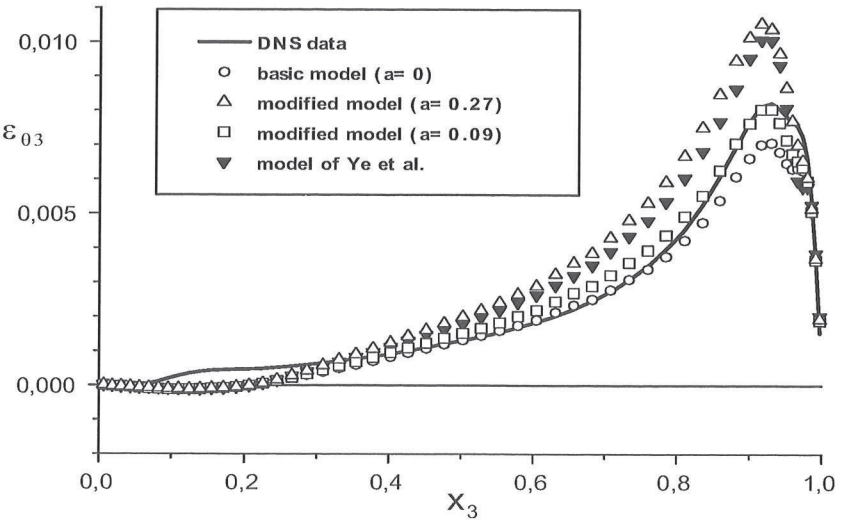

Figure 7. Comparison of models for $\varepsilon_{\theta 3}$ for internally heated convection.

6. Conclusions

A model is developed for the fluctuating temperature-gradient-velocity-gradient correlation, which appears in the buoyant production term in the dynamic dissipation rate equation and in the molecular sink term in the turbulent heat flux equation. Motivated by an analytical decomposition by the two-point correlation technique, the model is formulated consisting of an inhomogeneous and a homogeneous part. The inhomogeneous part is important near walls and needs no further modelling. For the homogeneous part a model is derived which incorporates the ratio Pr/R_h as key parameter. It is shown that for isothermal walls the model obeys the correct wall-limiting behaviour without explicit wall corrections. From comparisons with DNS data of natural convection in a horizontal fluid layer the excellent near-wall performance is confirmed for a wide range of Prandtl numbers. Using the DNS data, the homogeneuos part of the model is optimised by introducing a function $(Pr/R)^a$, where the exponent $a = a(Pr, Re_t + Pe_t)$ accounts for the Prandtl number and turbulence level. Towards the determination of a only a first step has been undertaken and further detailed investigations are needed.

While the performance of the model for the present DNS data of natural convection in horizontal fluid layers are very promising, the universality of the model needs to be shown. This requires the validation for other types of buoyant flows, e.g. natural convection in a differentially heated vertical channel. Here, the DNS data of Versteegh and Nieuwstadt [5] could be used. Dol et al. [2] proposed a model for $\varepsilon_{\theta i}$ and tested it against the DNS data of [5]. They use a wall function in terms of the invariant of the Reynolds stress anisotropy tensor, and a full differential or algebraic stress model is required. The performance of their model for the present DNS data will be investigated in future.

The present model for $\varepsilon_{\theta i}$ and $P_{\varepsilon b}$ shows a good performance, in particular near walls, while it is much simpler than models for these terms available in literature. This makes it attractive for implementation in engineering CFD codes to be applied to flows dominated by buoyancy. It can also be used when a second moment closure for $\overline{\theta u_i}$ is combined with a $k - \varepsilon$ model, instead of a full Reynolds stress model. Such a mixed first/second order model for turbulent momentum/heat transfer is used in our FLUTAN code.

REFERENCES

1. P.Y. Chou, Quart. Appl. Math., 3 (1945) 38.
2. H.S. Dol, K. Hanjalić & S. Kenjereš, Int. J. Heat and Fluid Flow, 18 (1997) 4.
3. B.A. Kolovandin & I.A. Vatutin, Int. J. Heat Mass Transfer, 15 (1972) 2371.
4. N. Shikazono & N. Kasagi, Int. J. Heat Mass Transfer, 39 (1996) 2977.
5. T.A.M Versteegh & F.T.M. Nieuwstadt, In *Turbulence, Heat and Mass Transfer 2*, Eds.: K. Hanjalić & T.W.J. Peeters, Delft University Press (1997) 471.
6. G. Willerding & W. Baumann, Forschungszentrum Karlsruhe, FZKA 5712 (1996).
7. M. Wörner, M. Schmidt & G. Grötzbach, J. Hydraulic Research, 35 (1997) 773.
8. Q.-Y. Ye, M. Wörner, G. Grötzbach & J. Jovanović, In *Turbulence, Heat and Mass Transfer 2*, Eds.: K. Hanjalić & T.W.J. Peeters, Delft University Press (1997) 331.
9. Q.-Y. Ye, M. Wörner & G. Grötzbach, Forschungszentrum Karlsruhe, FZKA 6103 (1998).
10. http://www.fzk.de/IRS/eng/IRS3/TURBIT_DNS_database.html.